Observations of Transition Phenomena on a Controlled Diffusion Compressor Stator With a Circular Arc Leading Edge

Alan D. Henderson[1]
e-mail: alan.henderson@utas.edu.au

Gregory J. Walker
e-mail: greg.walker@utas.edu.au

School of Engineering,
University of Tasmania,
Private Bag 65,
Hobart 7001, Australia

Laminar-turbulent transition behavior is studied near the leading edge of an outlet stator blade in a low-speed 1.5-stage axial-flow research compressor. The stator is a typical controlled diffusion design with a circular arc leading edge profile. Slow-response surface pressure distribution measurements are compared with numerical predictions from the quasi-two-dimensional flow solver, MISES. These both show a strong flow acceleration around each side of the circular arc, followed by a rapid deceleration near each blend point of the arc to the main surface profile. The relative magnitude of the localized overspeeds varies significantly over the wide range of stator flow incidence investigated. The unsteady boundary layer behavior on the stator is studied using a midspan array of surface-mounted hot-film sensors. On the suction surface, wake-induced transitional and turbulent strips are observed to originate close to the leading edge. The boundary layer approaches separation near the leading edge blend point on the suction surface, but this does not always lead to localized turbulent breakdown or continuous turbulent flow: a significant portion of the flow on the forward part of the surface remains laminar between the wake-induced transitional strips. At high positive incidence the wake-induced transitional strips originate near the leading edge blend point, but their growth is suppressed by the strong flow acceleration. On the pressure surface, a small separation bubble forms near the leading edge blend point resulting in almost continuous turbulent flow over the whole incidence range studied. [DOI: 10.1115/1.3144163]

1 Introduction

The flow around a leading edge of an airfoil is known to significantly influence the downstream boundary layer development. The choice of leading edge geometry is therefore an important consideration in blade design. There are two types of leading edge geometry commonly used in axial turbomachinery blading: circular arc and elliptic. Walraevens and Cumpsty [1] and Tain and Cumpsty [2] discussed how circular arc leading edges offer a reasonable balance between acceptable performance and practical manufacturing tolerances. Leading edge radii of blades used in the core compressor of a large turbofan engine are typically 0.25–0.75% of chord [2]. A high-pressure compressor blade with a chord length of 20 mm may have a leading edge radius as small as 0.15 mm. Accurate manufacturing of leading edges this small is not practical without incurring great expense. In addition, there is evidence that ingestion of small particles during the normal life cycle of a gas turbine engine leads to erosion of blade leading edges that can substantially alter leading edge geometry and overall performance [3]. The discussion by Smith [4] to Walraevens and Cumpsty [1] indicates that it is not uncommon to encounter leading edges that are significantly blunter than circular in operating aircraft engines.

While circular arc leading edges may be common, they have some undesirable characteristics. The flow rapidly accelerates around the circular arc leading edge and then rapidly decelerates near the discontinuity in curvature that occurs at the blend point of the circular arc to the main surface. This rapid acceleration and deceleration of the flow appears as a localized "spike" in blade surface pressure distribution that is often referred to as a velocity "overspeed." The rapid deceleration is known to cause localized boundary layer separation with transition and turbulent reattachment [2]. Promotion of turbulent flow over most of a blade surface is undesirable both in terms of aerodynamic performance and blade row loss. However, as noted by Cumpsty [5], there is insufficient explanation of why leading edge spikes do not cause severe separation and a substantial increase in loss coefficient.

There have been several detailed studies of the flow over turbomachinery blades with circular arc leading edges. Sanger and Shreeve [6] studied a two-dimensional controlled diffusion (CD) stator in a cascade wind tunnel without wake disturbances. The stator was tested over an engine-representative range of Reynolds numbers (5×10^5–7×10^5). At low incidence, the suction surface (SS) boundary layer remained laminar to near midchord, where transition occurred through a small separation bubble. At near-design and positive incidences the suction surface boundary layer separated and reattached as a turbulent boundary layer very close to the leading edge ($x/c<0.05$). A sudden jump in transition location was expected to occur over a narrow incidence range, resulting in a substantial increase in profile loss from the increased momentum thickness; however, this was not observed in the measured pressure loss coefficient, which remained low and relatively constant over a range of incidence near the design point. Sanger and Shreeve [6] commented that realistic loss estimates near the design inlet flow angle could only be achieved by assuming the suction surface boundary layer had relaminarized in the accelerating flow region following the leading edge overspeed.

Hodson [7] studied the flow over a turbine blade section with a circular arc leading edge in a cascade wind tunnel. Flow visualization experiments showed that a small separation bubble formed on the suction surface near the leading edge. Measurements from surface-mounted hot-film sensors showed that the turbulent

[1]Corresponding author.

Contributed by the International Gas Turbine Institute of ASME for publication in the JOURNAL OF TURBOMACHINERY. Manuscript received May 29, 2008; final manuscript received February 21, 2009; published online March 24, 2010. Review conducted by David Wisler. Paper presented at the ASME Turbo Expo 2007: Land, Sea and Air (GT2007), Montreal, QC, Canada, May 14–17, 2007.

boundary layer immediately downstream of the bubble was relaminarized by the strong acceleration of the freestream flow. Hodson [7] claimed that the acceleration parameter K greatly exceeded the accepted threshold for relaminarization of 3.5×10^{-6}: Accelerations of this magnitude are common on the suction surfaces of turbine blades. That study demonstrates that a thin turbulent boundary layer near the leading edge of a turbomachine blade may be relaminarized by strong acceleration.

The use of an elliptic leading edge profile can avoid leading edge spikes at near-design incidence, as shown by Hobson et al. [8] and Halstead et al. [9]. However, the work of Walraevens and Cumpsty [1] and Liu et al. [10] suggest that separation bubbles will still form on blades with an elliptic leading edge profile at off-design incidences.

A recent study by Wheeler et al. [11] investigated the unsteady wake perturbed flow over a CD stator blade with a circular arc leading edge profile in a low-speed research compressor. Their study showed the flow around the leading edge to be strongly influenced by passing rotor wake disturbances. The boundary layer on the suction surface did not continuously separate or become fully turbulent at the leading edge; rather, turbulent spots appeared from within a locally thickened region of laminar boundary layer that resulted from an interaction between upstream rotor wake disturbances and the blade leading edge. Similar findings were made by Henderson et al. [12] in an independent study of wake-induced flow at a C4 stator blade leading edge. This suggests that the transition mechanism associated with unsteady wake interaction may well be independent of leading edge geometry. A numerical investigation by Henderson et al. [12] showed that the thickened laminar regions exhibited both higher shape factor and momentum thickness Reynolds number than in the undisturbed boundary layer. The resulting destabilization of the boundary layer contributed to the earlier appearance of both bypass and Tollmien–Schlicting (TS) wave packet phenomena on the blade surface.

The present study examines wake-induced flow at a compressor stator leading edge and subsequent flow development. The stator has a surface pressure distribution typical of controlled diffusion design with a circular arc leading edge profile. The time-mean surface pressure distribution is measured using a row of static pressure tappings. The results are compared with numerical simulations from the MISES flow solver of Drela and Giles [13]. Unsteady-flow phenomena occurring on the stator are studied with a row of surface-mounted hot-film sensors. The substantial effect of incidence on boundary layer development and wake-induced transition phenomena are discussed.

2 Experimental Detail

2.1 Research Compressor. The experimental measurements presented in this study were made in the low-speed research compressor at the University of Tasmania (UTAS). The facility comprises of a 1.5-stage axial compressor embedded in an open loop wind tunnel. Air enters the compressor radially through a cylindrical inlet with a diameter of 2.13 m and a width of 0.61 m. The flow passes through a 6.25:1 contraction, where it is turned through 90 deg to the axial direction. The compressor has three blade rows: inlet guide vanes (IGVs), rotor, and stator, as shown in Figs. 1 and 2. The IGV and rotor blade rows have 38 and 37 blades, respectively, giving respective solidities at midspans of $\sigma=1.01$ and $\sigma=0.980$. Both IGV and rotor blades are of British C4 section with a constant chord length of 76.2 mm and an aspect ratio of 3.0. The C4 blade section is described in Ref. [5].

A 38-blade C4 stator blade row used in previous studies [14,15,12] was replaced with a new stator with a circular arc leading edge, typical of CD design. The CD blade row was designed to reproduce the downstream flow field resulting from the C4 stator. The 152.4 mm chord length of the CD stator is double that of the C4 blades replaced; the number of CD blades was halved to 19 in order to maintain the same midspan solidity of $\sigma=1.01$. This longer chord length allowed testing at higher Reynolds numbers than previously possible. The axial space between rotor and stator blade rows was 18.4% of the stator chord length. The reduced frequency Ω of rotor wake disturbances experienced by the stator at design was 2.0.

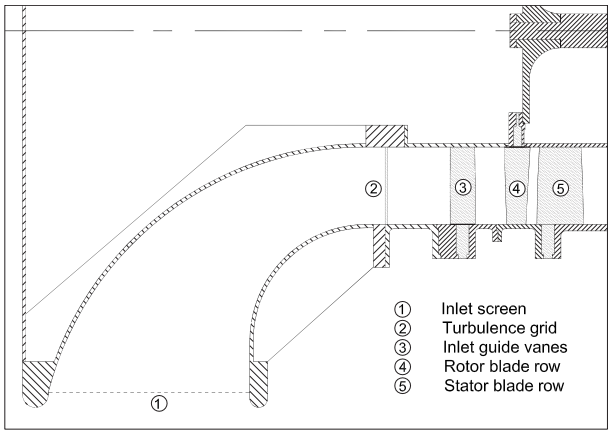

Fig. 1 UTAS research compressor cross section

The stator blades were molded out of a fast setting epoxy resin filled with aluminum powder. A steel support boss with reinforcing shank was inserted into each blade during the molding process. The maximum deviation from the design blade profile at midspan was less than ±0.2 mm.

All blade profiles were stacked about a radial axis to achieve free-vortex flow and 50% reaction at midspan position at design flow conditions. The test section annulus is constant in area with respective hub and casing diameters of 0.69 m and 1.14 m. Following the test section, the flow passes through a long annular diffuser before discharging through a cylindrical throttle at the exit. The throttle opening can be automatically adjusted to achieve the desired flow coefficient. The rotor is directly driven by a 30 kW dc motor. The speed is controlled by an analog feedback loop with a computer controlled reference voltage. The variation at a fixed setting is generally less than ±0.2 rpm. The speed was varied in response to changing atmospheric conditions to maintain constant Reynolds number operation during testing.

The background turbulence level of the research compressor was raised using a turbulence generating grid at the inlet, as described previously by Henderson et al. [15]. The turbulence grid was installed immediately downstream of the inlet contraction to allow mixing of rod wakes prior to the compressor stage. The grid consisted of 38 radial rods, each spanning between rings fixed to

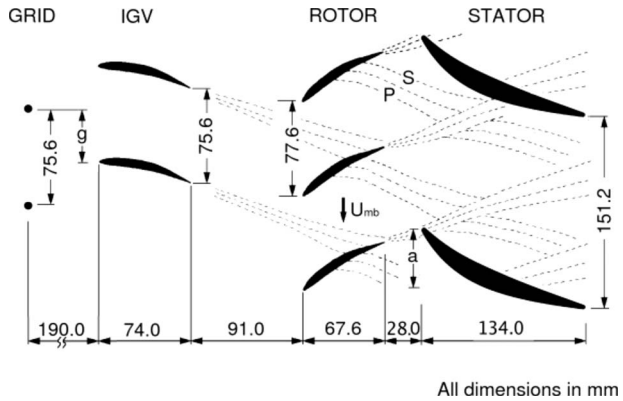

Fig. 2 Cross section of the research compressor showing the midspan blade row configuration with typical instantaneous wake dispersion pattern

Table 1 Stator operating conditions at midblade height

Incidence case	i (deg)	ϕ	Re_1	DF
A	−3.2	0.750	322,000	0.544
B	−1.2	0.710	315,000	0.613
C	0.5	0.675	308,000	0.671
D	3.3	0.610	293,000	0.758

the hub and casing. The number of rods was made equal to the number of blades in the IGV blade row so that every blade in a stator blade row would experience the same disturbance field. Instruments are inserted into the test section through an axial slot in the casing wall. A probe traversing rig allows accurate positioning in axial and radial directions. The IGV and stator blade rows are held in movable rings, which allow circumferential traversing (clocking) using stepper motors. The arrangement also permits relative circumferential traverses of the IGV and stator blade rows to be conducted with circumferentially fixed probes.

2.2 Scope of Investigation. Four incidence test cases were chosen to investigate the flow around the stator. These test cases, designated A–D, are detailed in Table 1. The time-mean stator incidence i was measured using a three-hole probe positioned in the center of the rotor-stator axial gap and slow-response instrumentation. A circumferential average was obtained by averaging 32 equally spaced measurement points over one stator blade pitch. The accuracy of this instrument in steady-flow conditions was estimated to be approximately ±0.2 deg.

All measurements were made at a constant reference Reynolds number of $Re_{ref}=160{,}000$ based on the rotor blade chord and peripheral velocity. The stator inlet Reynolds number (Re_1), based on the stator inlet velocity and chord, varies slightly with incidence as shown in Table 1, and satisfies the minimum Reynolds number proposed by Halstead et al. [16] for low-speed testing. Flow coefficient, stator chord Reynolds number, and Lieblein diffusion factor values are also shown for each test case. The IGV and rotor Reynolds numbers are considerably less than for the stator, owing to the shorter chord length, but are nonetheless above the critical Reynolds number for C4 blading (see Ref. [14]).

The corresponding Reynolds number based on leading edge radius (Re_r) is approximately 5700. Tain and Cumpsty [2] quoted typical values of Re_r for blades in a core compression system of a large aircraft engine at cruise conditions as $Re_r \approx 2600$ for the first stage rotor and $Re_r \approx 12{,}700$ for the last stage rotor. Most of the measurements given by Tain and Cumpsty [2] were performed at $Re_r \approx 12{,}000$.

The operating points for each test case are indicated on a the compressor characteristic shown in Fig. 3. Case A is at low incidence, Cases B and C are close to design, and Case D is at high incidence near the maximum pressure rise of the machine.

The turbulence level experienced by the stator was maintained between 2.0% and 3.0% by aligning the stator blade row in the IGV wake street ($a/S=0.0$). The measurements presented in Ref. [15] show that this configuration resulted in the most circumferentially uniform distribution of background turbulence.

2.3 Instrumentation and Measurement Techniques. One stator blade was instrumented with a midspan row of 39 slow-response static pressure tappings. Rectangular tracks 1 mm wide and 1.2 mm deep were machined into the surface at various positions around the blade. Polyethylene tubes with an external diameter of 1.05 mm and an internal diameter of 0.35 mm were laid into each track, and covered over with a fast setting polyester resin. The blade was lightly polished to achieve a uniform surface finish. A 0.5 mm diameter hole was machined into each tube at midspan. The average pressure at each tapping was determined by averaging readings sampled at 5 Hz over a 30 s period. The differential pressure measurements were made using a Datametrics Barocell 572 capacitive pressure transducer with a working range of ±13.3 kPa and accuracy of ±0.06% of reading. The accuracy of the surface velocity distribution U/U_{mb} values was estimated to be approximately ±0.9%.

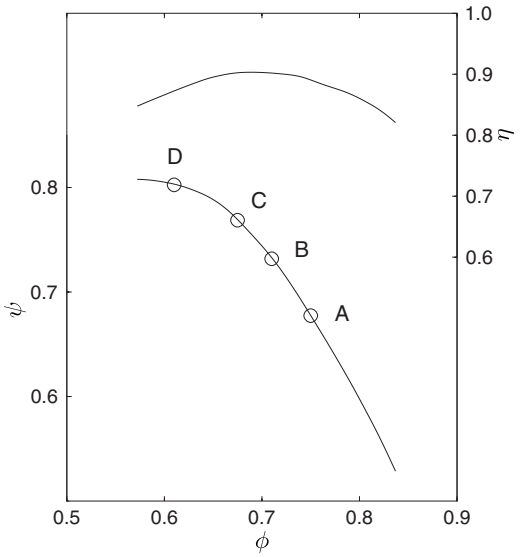

Fig. 3 Compressor performance characteristic showing test case operating points

A second stator blade was instrumented with an array of 74 surface-mounted hot-film sensors at midspan. The array was printed on three separate backing sheets: the first extended from the pressure surface (PS) trailing edge blend point, around the leading edge to $s^*=0.14$ on the suction surface; the second from $s^*=0.14$ to $s^*=0.56$ on the suction surface; and the third from $s^*=0.56$ to the suction surface trailing edge blend point. Care was taken to ensure a smooth transition between neighboring backing sheets. All sensors were a standard size of 1.44×0.1 mm and protruded a distance of 0.2 μm outwards from the blade surface. The sensor height was estimated to be approximately two orders of magnitude below the height of uniform roughness required to influence the transition Reynolds number on a flat plate (see Ref. [17]). A nonuniform sensor spacing was used to give higher spatial resolution around the leading edge (nine sensors between the leading edge blend points) and toward the trailing edge where turbulent separation may occur. A photograph of the instrumented blade is shown in Fig. 4.

The hot-film sensors were controlled with TSI-IFA100 constant temperature anemometers. The frequency response for each sensor was estimated to be better than 30 kHz. All signals were low pass filtered at 20 kHz and sampled at 50 kHz to avoid aliasing.

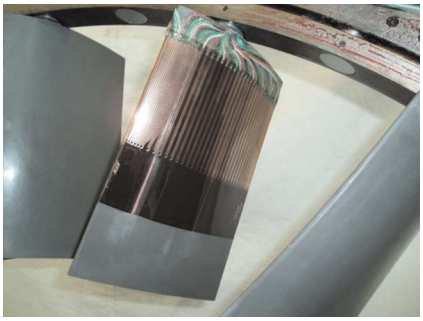

Fig. 4 Compressor blade instrumented with an array of hot-film sensors

Data acquisition was triggered once per revolution using an optical sensor with a reflective target fixed to a rotor blade tip. At each measurement station a maximum of five channels were simultaneously acquired 512 times, with each record containing 1024 sample points. Each record spans approximately eight rotor passing periods.

Measurements from hot-film sensors were processed to yield quasiwall shear stress using a method developed by Hodson et al. [18]. The quasiwall shear stress is approximately proportional to wall shear stress, as expressed by

$$\tau_q = \left(\frac{E^2 - E_o^2}{E_o^2} \right)^3 \propto \tau_w \tag{1}$$

This approach has been used in numerous studies, including Refs. [9,14,15,12].

The quasiwall shear stress measurements were interpreted for laminar, turbulent, or relaxing flow using a method developed by Solomon [19]. This method was based on an intermittency detection algorithm that used both probability density functions (PDFs) and peak-valley counting (PVC). Individual records were then averaged to yield the temporal variation of ensemble-averaged turbulent intermittency $\langle \gamma \rangle$. The PVC/PDF method of Solomon [19] is highly automated, requiring little user input. Walker et al. [14] presented results showing both ensemble-averaged quasiwall shear stress and ensemble-averaged intermittency, finding the latter to give a more useful description of the state of the boundary layer.

3 Numerical Method

The quasi-three-dimensional steady-flow solver, MISES, of Drela and Giles [13] was used to calculate the flow through the stator blade row. This was done for several reasons. The simulations provide confirmation of the incidence measurements made using the three-hole probe, and highlight the strong two-dimensionality of the flow at midspan position. It is of general interest to engine designers to know how well design and analysis codes model actual flow behavior.

The MISES flow solver, which is commonly used in industry as a preliminary design tool, solves both the inviscid Euler equations and a set of integral boundary layer equations simultaneously using a Newton method. The onset of transition to turbulent flow is determined using a hybrid method that combines a bypass transition correlation with a linear stability theory method. Transition onset occurs by the first method to detect transition. A detailed description of the code is given in Ref. [13]. The MISES flow solver has been well validated and used in numerous earlier studies [20,2,21]. MISES version 2.4 was used for the present work.

The prescribed level of inlet turbulence influences the location where transition will occur on the blade surface and the subsequent boundary layer development. Simulations were performed at inlet turbulence intensities of 1% and 3%, the latter being approximately equal to the background level of turbulence intensity measured in the research compressor. As discussed later, the 1% Tu calculation better captures the detail of leading edge separation behavior. In each test case, the flow incidence was set to the measured values given in Table 1.

4 Surface Velocity Distributions

The stator midspan surface velocity distributions for test cases A–D are shown in Fig. 5. Slow-response surface pressure tappings' measurements are compared with numerical simulations from the MISES flow solver.

The close agreement between the measured and calculated surface pressure distributions indicates that the measured inlet flow angle is accurate to within ± 0.5 deg. Although the MISES solutions are expected to differ slightly from the experimental results, primarily due to unsteady and three-dimensional flow effects, the calculations provide useful information about the effect of incidence on flow behavior.

The overall shape of the velocity distributions is typical of controlled diffusion design. Following the leading edge overspeed, the flow on the suction surface accelerates to a peak velocity located near $s^* = 0.25 - 0.30$. This is followed by a deceleration that gradually decreases in strength toward the trailing edge to reduce the likelihood of turbulent separation.

Leading edge overspeeds are clearly evident on both the suction and pressure surfaces. The high level of detail around the leading edge is not evident in Fig. 5. To show this more clearly, the data around the leading edge have been replotted over a smaller surface distance in Fig. 6. The maximum overspeed velocity occurs slightly upstream from the blend points, as also noted by Tain and Cumpsty [2] in their study of a low Mach number flow over a flat plate airfoil with a circular arc leading edge profile.

The height of the suction surface overspeed increases with positive incidence and the height of the pressure surface overspeed decreases with positive incidence. The height of the suction surface overspeed is found to have a large influence on the boundary layer development predicted by the MISES flow solver. In Cases A ($i = -3.2$ deg) and B ($i = -1.2$ deg) at Tu = 1%, the destabilization caused by the leading overspeed is not sufficient to cause transition to be predicted at the leading edge. Instead, separated flow transition occurs further along the surface near $s^* \approx 0.5$ and $s^* \approx 0.4$, respectively. As incidence is increased in Case C ($i = 0.5$ deg), the height of the suction surface overspeed increases and transition is predicted at the leading edge via a small separation bubble. Further increasing incidence to Case D ($i = 3.3$ deg) increases the size of the separation bubble, and a characteristic perturbation appears in the predicted velocity distribution. The corresponding experimental surface pressure distributions lack sufficient spatial resolution to confirm the existence of separation bubbles.

In Case D, the velocity distribution levels out toward the trailing edge. This poor pressure recovery indicates that the turbulent boundary layer is close to separation there. The MISES flow solver predicts turbulent separation at $s^* = 0.9$. Here, the experimental results are expected to differ to some extent due to changing axial velocity–density ratio (AVDR) caused by three-dimensional flow effects from endwall and corner flows.

The flow on the pressure surface experiences a greater deceleration near the leading edge than on the suction surface. This is followed by a mild acceleration to the trailing edge. Cases A–C show a discontinuity in the measured surface velocity gradient following the pressure surface blend point. This indicates the presence of a separation bubble, as also predicted in solutions from the MISES flow solver.

The size of the leading edge separation bubbles and their associated influence on surface velocity are strongly related to the specified level of inlet turbulence: Increasing the inlet turbulence intensity from 1% to 3% decreases the predicted spatial distance to transition onset. As a consequence, the transition location for Case B moves to the leading edge and for Case A moves upstream to $s^* \approx 0.3$. Increasing the prescribed turbulence intensity decreases the size of the leading edge separation bubbles, which consequently results in a smaller perturbation in the surface velocity distribution. The lower turbulence intensity of 1% gives better agreement with the experimental results around the leading edge due to a tendency for the MISES solver to overpredict the rate of increase in turbulent shear stress following the transition point (see Ref. [22]).

The time-average observations of unsteady surface pressures presented in this section must be expected to differ somewhat from the steady-flow solutions from the MISES flow solver. A time-resolved simulation of the flow past a CD stator by Wheeler et al. [11] showed that the height of the leading edge overspeeds changed significantly with the wake passing phase. A numerical simulation of the CD stator used in this study (not presented here)

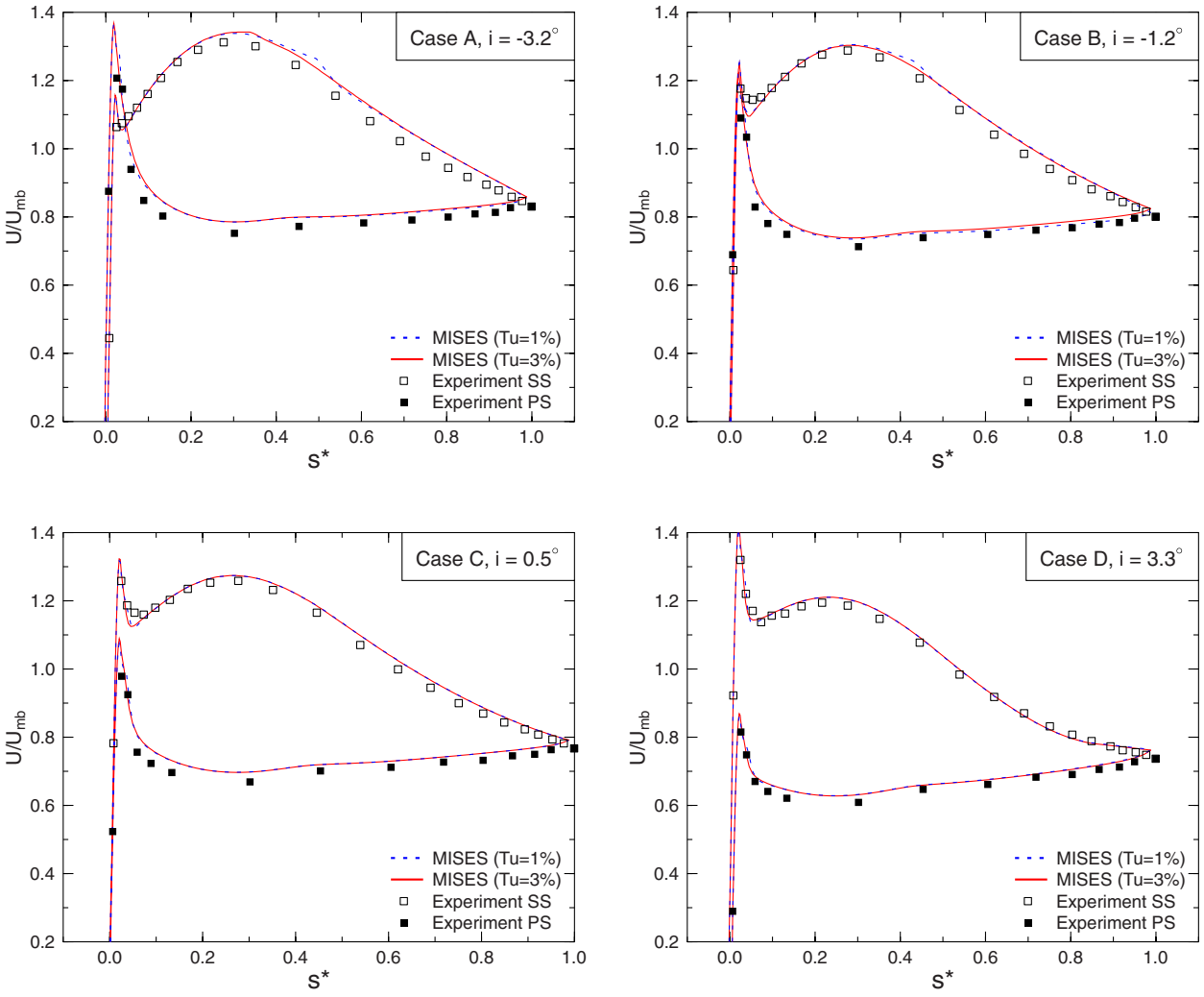

Fig. 5 Stator surface velocity distributions: experimental results and MISES predictions

was also performed using the UNSFLO flow solver in a similar manner to Henderson et al. [12] and Wheeler et al. [11]. This predicted a small periodic region of laminar separation in the decelerating flow at the suction surface overspeed. The tendency for periodic separation was observed to increase with incidence, as the height of the leading edge overspeed increased.

The time-resolved hot-film measurements presented in Sec. 5 provide more detailed information on the unsteady-flow phenomena occurring on the blade surface near the leading edge.

5 Hot-Film Surveys

Data from all 74 hot-film sensors were recorded and then interpreted to determine ensemble average turbulent intermittency and probability of relaxing flow in calmed regions following the occurrence of turbulent flow, as shown in Fig. 7. In addition, two sets of representative measurements from five hot-film sensors on each side of the blade are presented in Fig. 8. The measurements in each set were recorded simultaneously. The position of each sensor is indicated on the right-hand side of Fig. 8. These figures are now discussed to interpret the unsteady-flow phenomena occurring on each blade surface.

5.1 Suction Surface. The gray shaded contours of ensemble average intermittency in Fig. 7 show that the flow on the suction surface is dominated by wake-induced transitional strips not unlike those observed in other studies [14,9,11]. However, the character of the transitional strips for the high incidence Case D differs from that at lower incidences.

In Cases A–D, short intense bursts of turbulent flow were detected very close to the leading edge ($s^* \approx -0.02$ and $s^* \approx 0.02$). Their relative timing coincides with the arrival of the rotor wake at the leading edge of the stator blade. These are unlikely to be turbulent spots given the strong acceleration of the flow and the low momentum thickness Reynolds number. The most likely explanation is that the thin boundary layer is buffeted by the strong turbulence, and vortical and pressure disturbances associated with the passing wake, which leads to false detection of turbulent flow. These events have been used as the origin of overlaid particle trajectories traveling at several fractions of the freestream flow: $1.0U$, $0.88U$, $0.7U$, and $0.5U$.

A second localized detection of turbulence occurs further along the suction surface, in decelerating flow following the leading edge overspeeds. These disturbances are shown in the raw hot-film measurements near $s^*=0.095$ in Fig. 8 as indicated by event "1." Several types of flow phenomena may be responsible. The disturbances may be small turbulent spots, turbulent spots that have partially relaminarized, or "puff" phenomena that eventually cause turbulent spots when conditions allow. The mean convection speed of puff type disturbances is similar to that of turbulent spots ($0.7U$), which makes them difficult to distinguish from turbulent spots [23]. However, in Case D, the significant levels of calming and intermittency detected near $s^*=0.095$ suggest that genuine turbulent breakdown has occurred.

A likely mechanism for the formation of these structures was

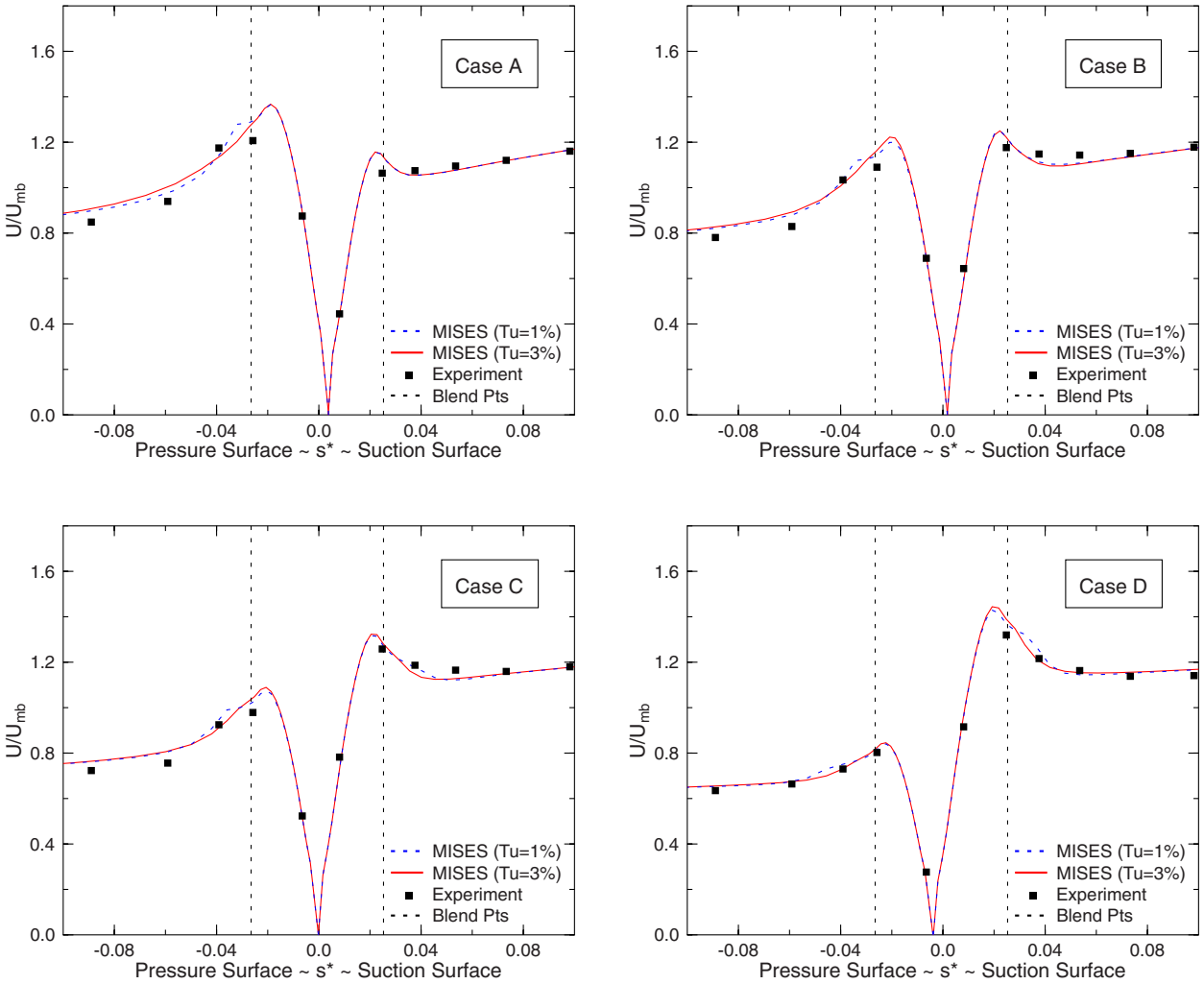

Fig. 6 Stator surface velocity distributions around the leading edge: experimental results and numerical predictions from the MISES flow solver

provided in recent studies by Henderson et al. [12] and Wheeler et al. [11]. As a rotor wake disturbance interacts with a stator blade boundary layer, it produces a thickened laminar flow structure in the suction surface boundary layer that convects at approximately $0.7U$. The structure is characterized by both elevated momentum thickness Reynolds number and boundary layer shape factor, both of which have a destabilizing effect on the boundary layer, leading to the formation of turbulent spots and bypass transition phenomena. The thickened laminar flow structures are evident in the raw hot-film data shown near $s^* \approx 0.032$ in Fig. 8 as periodic decreases in quasiwall shear stress (see event "3").

The suction surface boundary layer behavior is strongly influenced by incidence. In Case A, the leading edge pressure spike is relatively small and following it, the boundary layer experiences a strong favorable pressure gradient. The raw hot-film records shown in Fig. 8 show flow structures traveling along the surface, some of which develop into turbulent spots (see event "2"), while others decay (see event "1"). Increasing incidence also increases the level of destabilization at the leading edge, and this correspondingly increases the periodicity of turbulent flow events. A local boundary layer separation may be responsible for the rapid appearance of well developed turbulent spots near $s^* \approx 0.095$ in Case D (see events "4" and "5").

Wake-induced transitional strips occur on the suction surface for all the cases shown in Fig. 7. In incidence Cases A–C, the leading and trailing edges of the strips are approximately parallel to overlaid particle trajectories at $0.88U$ and $0.5U$. This is generally consistent with the envelope of wake-induced transitional strips observed in other studies of transitional flow on compressor blades [14,9], and agrees with experimental measurements of turbulent spots in flows with an adverse pressure gradient [24].

The turbulent spots observed near the leading edge in Case D do not grow as spots in flows with a zero or adverse pressure gradient, where leading and trailing edges travel at speeds of approximately $0.9U$ and $0.5U$, respectively (see Refs. [9,14]). Inspection of the raw hot-film records shows that some spots grow (see event 5), while others appear to decay (see event 4). This observation is supported by the slight reduction in width of the wake-induced transitional strips between $0.06 < s^* < 0.2$ shown in Fig. 7. The elevated level of turbulent intermittency between wake induced transitional strips ($\langle \gamma \rangle \approx 0.5$) is due to intermittent appearances of larger regions of turbulent flow. The wide variety of phenomena observed in the data makes it difficult to make firm conclusions; however, the growth of turbulent spots clearly appears to be significantly affected by the favorable pressure gradient. Nonetheless, the leading and trailing edge celerities of the wake-induced transitional strips between $0.1 < s^* < 0.4$ remain approximately constant at $0.7U$. Experiments have shown that the spot spreading angle reduces with increasingly favorable pressure gradient (see Refs. [24,25]). The calculated acceleration parameter in Fig. 9 for Cases A and B shows that the acceleration parameter

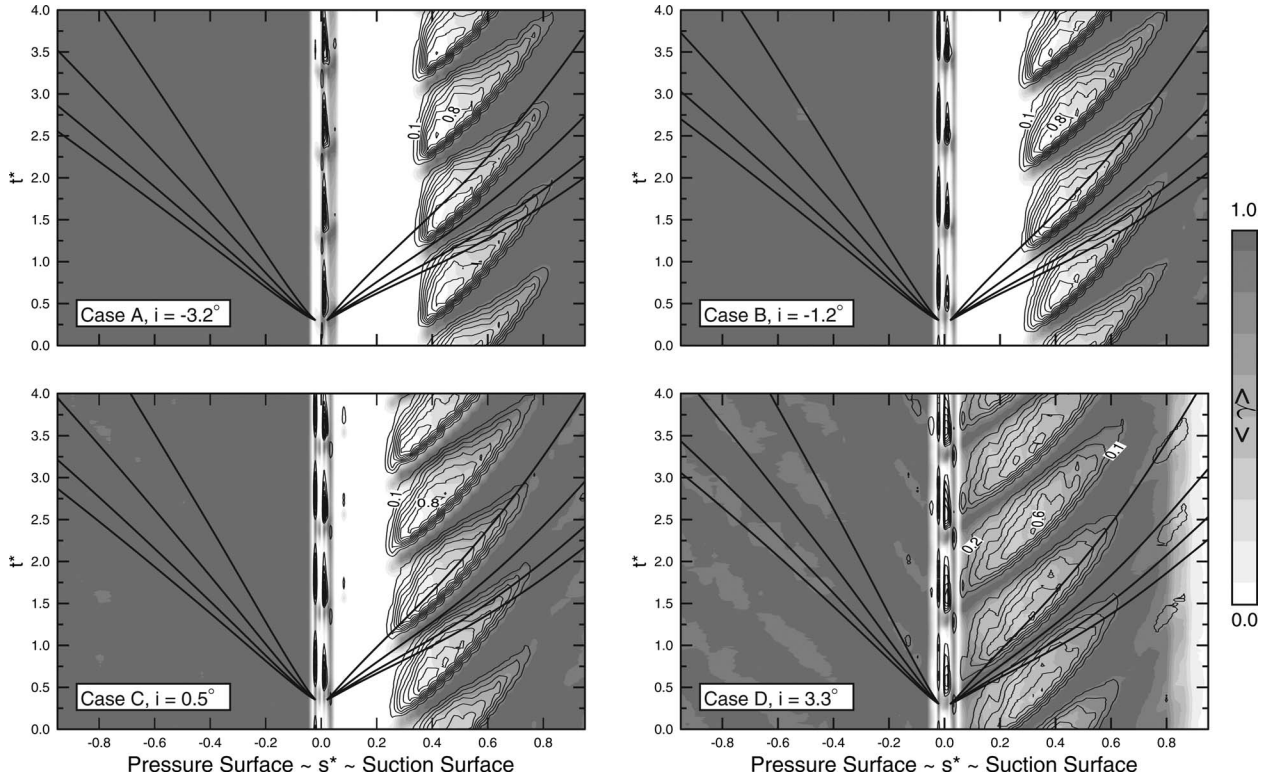

Fig. 7 CD stator surface intermittency distributions for Cases A–D. Color contours show ensemble average intermittency $\langle\gamma\rangle$, line contours show probability of calmed flow in intervals of 0.1, and lines show particle trajectories at 1.0*U*, 0.88*U*, 0.7*U*, and 0.5*U*.

exceeds the accepted level $K \approx 3.0\times10^{-6}-3.5\times10^{-6}$ required to relaminarize a fully turbulent boundary layer. It is well known that relaminarization of a fully turbulent boundary layer is not instantaneous and requires acceleration over a suitable length to complete [26], but there is little available information on the effects of very strong acceleration on isolated turbulent spots. The boundary layer momentum thickness Reynolds number shown in Fig. 9 indicates that low Reynolds number effects are also likely to be important and may contribute to the observed damping of turbulent spots [26].

In Cases A–C, wake-induced transitional strips do not appear in the ensemble average intermittency until further along the surface ($s^*>0.25$) despite the presence of disturbances shown in the raw hot-film data of Fig. 8. Although not evident in this figure, low levels of ensemble average intermittency are detected from near the leading edge to where significant levels of intermittency occur. There are several likely explanations for this. The PVC/PDF algorithm will only detect turbulent flow if high frequency fluctuations occur over within a set window period; most of the disturbances observed near the leading edge do not have such a sustained period of fluctuation and are not identified as turbulent. The variability in arrival time of passing rotor wakes (or "phase jitter") may also contribute to low levels of ensemble average intermittency. Nonetheless, the majority of disturbances observed near the leading edge travel at a mean convection speed of $0.7U$, and eventually develop into the wake-induced transitional strips shown in Fig. 7. This identifies the leading edge as the key receptivity site for wake-induced transition on the suction surface of CD type compressor blades.

Case D shows a decrease in turbulent intermittency toward the trailing edge. The low level of intermittency does not necessarily indicate separation, although this was predicted in solutions from the MISES flow solver. This decrease in intermittency may be due to the reduced ability of the PVC/PDF algorithm to detect turbulent flow in decelerating flows with low levels of wall shear stress. Replotting Fig. 7 with a lower intermittency scale shows that wake-induced transitional strips continue to travel along the surface, which suggests that complete boundary layer separation may not have occurred. However, it should be noted that turbulent separation is an unsteady process, so forward flow will be intermittently observed upstream of the time-mean separation point.

A region of calmed flow follows each wake-induced transitional strip as shown by the line contours of calmed flow probability. Calmed flow is identified when the shear stress continuously falls following detection of a turbulent event. Detection of calmed flow is terminated by the first subsequent increase in shear stress. In most of the test cases, regions of relaxing flow are terminated by the arrival of the next wake-induced transitional strip. This makes it highly likely that different flow behaviors would occur at lower reduced frequency, as shown by Halstead et al. [9] and Solomon [19].

5.2 Pressure Surface. The intermittency distribution on the pressure surface is generally less sensitive to incidence than on the suction surface. The high level of intermittency ($\langle\gamma\rangle=0.9$) indicates almost completely turbulent flow in most cases. The boundary layer is separated at $s^*=-0.032$ in all cases, as evidenced from the very low levels of quasiwall shear stress, marked by an occasional flow event. Turbulent reattachment occurs near $s^*=-0.10$, as indicated by the rapid rise in intermittency following the blend point. A weak calming effect is observed near the leading edge in the high incidence Case D, as indicated by a lower level of intermittency accompanied with a low probability detection of laminar flow. Further confirmation that this a genuine calmed flow region is provided by an observed celerity of approximately $0.5U$. This flow phenomenon was also observed by Walker et al. [14] on the pressure surface of C4 stator blade at low incidence. If a wake-induced transitional strip develops slightly upstream of the separation point of the undisturbed flow, the calmed region following the strip may temporarily suppress the separation bubble.

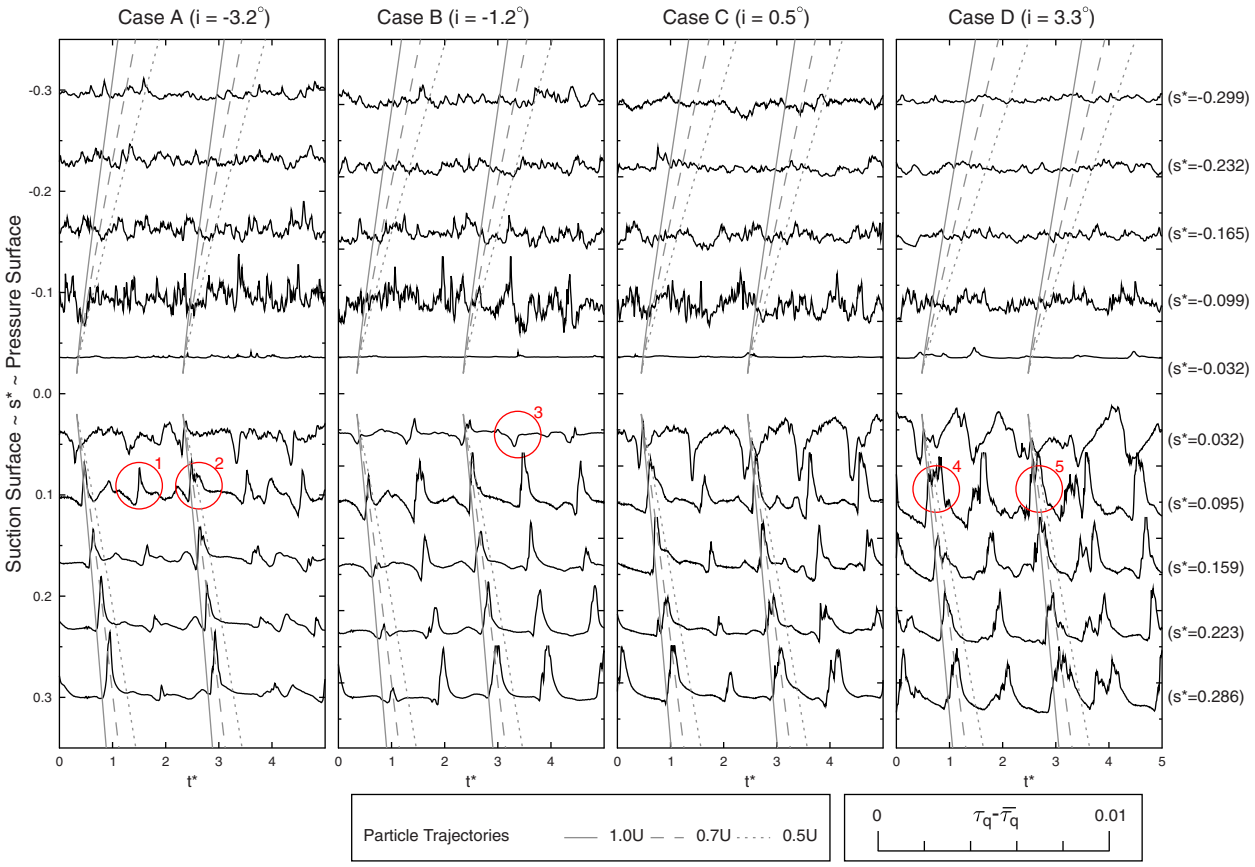

Fig. 8 Typical raw quasiwall shear stress records near the stator leading edge

Case D also shows a temporal variation of intermittency further along the surface ($-0.97 < s^* < -0.40$) as indicated by bands with lower intermittency ($0.8 < \langle\gamma\rangle < 0.9$) than in the surrounding flow. These are caused by intermittent regions of calmed flow that develop further along the surface. This variation travels at speed close to $1.0U$, which suggests that it is caused by buffeting of the boundary layer by passing rotor wakes, although the intermittent suppression of the leading edge separation bubble could also have contributed.

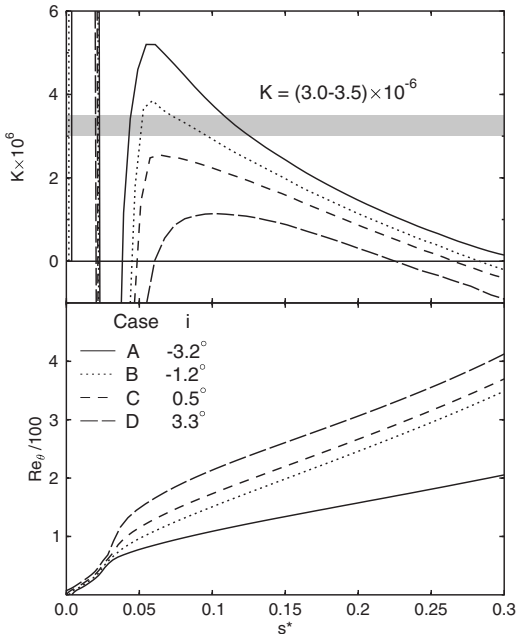

Fig. 9 Predicted suction surface acceleration parameter and momentum thickness Reynolds number (MISES) for Tu=3%

6 Conclusions

Transitional flow near the circular arc leading edge of a CD stator in a 1.5-stage axial compressor has been investigated at midspan. Numerical simulations from the MISES steady-flow solver and experimental results from slow-response pressure tappings reveal large flow overspeeds near the leading edge blend points. The height of the suction surface leading edge overspeed increases with incidence. This is shown to cause a greater destabilization of the suction surface boundary layer with separated flow transition predicted at the leading edge.

Unsteady wake-induced transition near the stator leading edge was investigated using a row of surface-mounted hot-film sensors. These measurements showed that the flow on the suction surface was not completely turbulent at positive incidence, as predicted by steady-flow calculations using the MISES solver. Instead, a complex flow pattern of wake-induced transitional strips and calmed flow was observed, with evidence of turbulence decay or relaminarization in some circumstances. This clearly indicates that the suction surface flow cannot not be accurately modeled using a fully turbulent assumption.

Periodic turbulent spots and flow disturbances occurred on the suction surface very close to the leading edge ($s^* \approx 0.1$) at time intervals corresponding to the arrival of upstream rotor wakes. These were observed in all test cases, although the periodicity of turbulent spots increased with incidence. The majority of flow disturbances traveled with a mean speed of $0.7U$, eventually growing to form classic wake-induced transitional strips. The fact that these originated near the leading edge again points to the

leading edge as the principal receptivity site for wake-induced bypass transition on the suction surface of compressor blades as shown in recent studies [12,11].

The strong favorable pressure gradient on the suction surface following the leading edge overspeed appeared to have a stabilizing effect on the boundary layer, slowing the growth of turbulent spots propagating along the surface.

A small leading edge separation bubble formed after the pressure surface overspeed, resulting in turbulent flow over the remainder of the surface. Periodic variations in turbulent intermittency were observed to travel along the pressure surface traveling at about the freestream velocity. This appears consistent with buffeting of the boundary layer by passing rotor wakes.

Acknowledgment

The authors gratefully acknowledge the financial assistance from Rolls-Royce plc. The reviewers of this paper are thanked for helpful comments.

Nomenclature

a = circumferential distance of stator blade leading edge from the center of IGV wake street at midspan
c = blade chord
E = anemometer output voltage
E_0 = anemometer output voltage at zero flow
i = blade incidence, α-β
K = acceleration parameter, $(\nu/U^2)dU/ds$
r = leading edge radius
$\mathrm{Re}_{\mathrm{ref}}$ = reference Reynolds number (rotor chord), $U_{mb}\cdot c/\nu$
Re_r = leading edge Reynolds number, $V_1\cdot r/\nu$
Re_1 = stator inlet Reynolds number (stator chord), $V_1\cdot c/\nu$
s = surface length from the leading edge
$s_{\max}$ = surface length from the leading edge to the trailing edge
s^* = dimensionless surface length, $s/s_{\max}$
S = blade pitch
t = time
t^* = dimensionless time, t/T
T = rotor blade passing period
Tu = random disturbance level (turbulence)
U = local freestream velocity
U_{mb} = midspan rotor blade speed
V_a = mean axial velocity at compressor inlet
V_1 = velocity at stator inlet
α = stator inlet flow angle
β = stator inlet blade angle
γ = turbulent intermittency
η = overall efficiency
θ = boundary layer momentum thickness
ν = kinematic viscosity
ρ = air density
σ = solidity, c/S
τ_q = quasiwall shear stress
τ_w = wall shear stress
ϕ = flow coefficient, V_a/U_{mb}
ψ = pressure coefficient, $2\Delta P/\rho U_{mb}^2$
ω = blade passing frequency
Ω = reduced frequency, $\omega c/V_1$

Superscripts, Subscripts, Abbreviations, etc.

DF = Lieblein diffusion factor for AVDR=1
$(\,)$ = time-mean
$\langle\,\rangle$ = ensemble (phase-lock) average
$(\,)^*$ = dimensionless quantity

References

[1] Walraevens, R. E., and Cumpsty, N. A., 1995, "Leading Edge Separation Bubbles on Turbomachine Blades," ASME J. Turbomach., **117**, pp. 115–126.
[2] Tain, L., and Cumpsty, N. A., 2000, "Compressor Blade Leading Edges in Subsonic Compressible Flow," Proc. Inst. Mech. Eng., Part C: J. Mech. Eng. Sci., **214**(1), pp. 221–242.
[3] Roberts, W. B., 1995, "Advanced Turbofan Blade Refurbishment Technique," ASME J. Turbomach., **117**, pp. 666–667.
[4] Smith, L. H., Jr., 1995, "Discussion: "Leading Edge Separation Bubbles on Turbomachine Blades" (Walraevens, R. E., and Cumpsty, N. A., 1995, ASME J. Turbomach., 117, pp. 115–125)," ASME J. Turbomach., **117**, pp. 125.
[5] Cumpsty, N. A., 1989, *Compressor Aerodynamics*, Longman Scientific and Technical, Essex, UK.
[6] Sanger, N. L., and Shreeve, R. P., 1986, "Comparison of Calculated and Experimental Cascade Performance for Controlled-Diffusion Compressor Stator Blading," ASME J. Turbomach., **108**, pp. 42–50.
[7] Hodson, H. P., 1985, "Boundary-Layer Transition and Separation Near the Leading Edge of a High-Speed Turbine Blade," ASME J. Eng. Gas Turbines Power, **107**, pp. 127–134.
[8] Hobson, G., Hansen, D., Schnorenberg, D., and Grove, D., 2001, "Effect of Reynolds Number on Separation Bubbles on Compressor Blades in Cascade," J. Propul. Power, **17**(1), pp. 154–162.
[9] Halstead, D. E., Wisler, D. C., Okiishi, T. H., Walker, G. J., Hodson, H. P., and Shin, H.-W., 1997, "Boundary Layer Development in Axial Compressors and Turbines: Part 2 of 4—Compressors," ASME J. Turbomach., **119**(3), pp. 426–444.
[10] Liu, H., Liu, B., Li, L., and Jiang, H., 2003, "Effect of Leading-Edge Geometry on Separation Bubble on a Compressor Blade," ASME Paper No. GT-2003-38217.
[11] Wheeler, A. P. S., Miller, R. J., and Hodson, H. P., 2006, "The Effect of Wake-Induced Structures on Compressor Boundary Layers," ASME Paper No. GT2006-90892.
[12] Henderson, A. D., Walker, G. J., and Hughes, J. D., 2006, "Unsteady Transition Phenomena at a Compressor Blade Leading Edge," ASME Paper No. GT2006-90641.
[13] Drela, M., and Giles, M. B., 1987, "Viscous-Inviscid Analysis of Transonic and Low Reynolds Number Airfoils," AIAA J., **25**(10), pp. 1347–1355.
[14] Walker, G. J., Hughes, J. D., and Solomon, W. J., 1999, "Periodic Transition on an Axial Compressor Stator: Incidence and Clocking Effects: Part I—Experimental Data," ASME J. Turbomach., **121**, pp. 398–407.
[15] Henderson, A. D., Walker, G. J., and Hughes, J. D., 2006, "Influence of Turbulence on Wake Dispersion and Blade Row Interaction in an Axial Compressor," ASME J. Turbomach., **128**(1), pp. 150–157.
[16] Halstead, D. E., Wisler, D. C., Okiishi, T. H., Walker, G. J., Hodson, H. P., and Shin, H.-W., 1997, "Boundary Layer Development in Axial Compressors and Turbines: Part 1 of 4—Composite Picture," ASME J. Turbomach., **119**(1), pp. 114–127.
[17] Schlichting, H., 1968, *Boundary-Layer Theory*, 6th ed., McGraw-Hill, New York.
[18] Hodson, H. P., Huntsman, I., and Steele, A. B., 1994, "An Investigation of Boundary Layer Development in a Multistage LP Turbine," ASME J. Turbomach., **116**(3), pp. 375–383.
[19] Solomon, W. J., 1996, "Unsteady Boundary Layer Transition on Axial Compressor Blades," Ph.D. thesis, University of Tasmania, Australia.
[20] Solomon, W. J., Walker, G. J., and Hughes, J. D., 1999, "Periodic Transition on an Axial Compressor Stator: Incidence and Clocking Effects: Part II—Transition Onset Predictions," ASME J. Turbomach., **121**, pp. 408–415.
[21] Köller, U., Mönig, R., Küsters, B., and Schreiber, H. A., 2000, "Development of Advanced Compressor Aerofoils for Heavy-Duty Gas Turbines: Part 1—Design and Optimization," ASME J. Turbomach., **122**, pp. 397–405.
[22] Drela, M., and Youngren, H., 1998, "A User's Guide to MISES 2.53," MIT Computational Aerospace Sciences Laboratory, Technical Report.
[23] Boiko, A. V., Grek, G. R., Dovgal, A. V., and Kozlov, V. V., 2002, *The Origin of Turbulence in Near-Wall Flows*, Springer, Berlin.
[24] D'Ovidio, A., Harkins, J. A., and Gostelow, J. P., 2001, "Turbulent Spots in Strong Adverse Pressure Gradients. Part 2—Spot Propagation and Spreading Rates," ASME Paper No. 2001-GT-406.
[25] Zhong, S., Chong, T. P., and Hodson, H. P., 2003, "A Comparison of Spreading Angles of Turbulent Wedges in Velocity and Thermal Boundary Layers," ASME J. Fluids Eng., **125**, pp. 267–274.
[26] Warnack, D., and Fernholz, H. H., 1998, "The Effects of a Favourable Pressure Gradient and of the Reynolds Number on an Incompressible Axisymmetric Turbulent Boundary Layer. Part 2. The Boundary Layer With Relaminarization," J. Fluid Mech., **359**, pp. 357–381.